PERFORMANCE ANALYSIS OF RADAR TARGET RECOGNITION USING NATURAL FREQUENCY: FREQUENCY DOMAIN APPROACH

J.-H. Lee[1, *], S.-W. Cho[1], S.-H. Park[2], and K.-T. Kim[3]

[1]Department of Information and Communication Engineering, Sejong University, Seoul, Korea

[2]Department of Electronic Engineering, Pukyong National University, Busan, Korea

[3]Department of Electronic Engineering, Pohang University of Science and Technology, Pohang, Korea

Abstract—We consider the performance analysis of natural frequency-based radar target recognition in the frequency domain. Based on the probability density function (PDF) of some quantity consisting of the projections of the frequency response onto the column spaces of the matrices constructed using the natural frequencies of the specific targets, we propose to analytically calculate the probability of the correct classification, where the PDF is obtained from the inverse Fourier transform of the characteristic function. The scheme is validated by comparing the performance using the analytic method with that using the Monte-Carlo simulation.

1. INTRODUCTION

Radar [1–13] has been a sensor for detection [14–25] and tracking [13, 26] of the target. Traditionally, radar can measure the range to the target and the velocity of the target. Conceptually, the velocity of the moving target can be estimated based on the Doppler shift [14, 22, 23, 27–29]. In addition, from the strength of the signal reflected from the target, the radar cross section (RCS) [9, 10, 30–35] of the target can be estimated. However, there parameters give only a rough estimate of the general category of the actual target type. The reflected signal of the radar target can be simulated using scattering

analysis of the radar target [36–49]. In addition to radar detection and tracking, there have been mamy studies on radar target recognition [3, 7, 50–59, 61–70]. The expressions of recognition, classification and identification have been used interchangeably.

Radar target recognition is achieved using radar signatures, like natural frequencies of the radar target [60–64, 67–70] high resolution range (HRR) profiles [52, 57–59, 71] of the radar target and microwave image of the radar target [1–4, 14, 24, 28, 34, 50, 53, 72–83]. Inverse synthetic aperture radar (ISAR) images [3, 21, 34, 78–83] has been one of the most popular microwave imaging techniques for radar target recognition. Useful features used for target recognition also include jet engine modulation [84] and helicopter [12, 86, 87] modulation.

It has been shown that the performance of radar target recognition can be improved by exploiting the polarization characteristics [1, 24, 49, 51, 55, 56, 76]. Recently, to detect low RCS [9, 10, 30–35] radar target, many studies have been conducted on MIMO radar, bistatic radar and multi-static radar [4, 18–20, 29, 43, 76–78, 85, 88–91]. To enhance the performance of the radar target recognition, pulse compression has also been adopted [92–94].

The performance of radar target recognition is dependent on the bandwidth of the transmitting signal of the radar. Therefore, ultra-wideband (UWB) radar [2, 5, 51, 82, 95] can be a good candidate for improving the performance of radar target recognition.

This paper is concerned with the performance analysis of the natural frequency-based radar target recognition in the frequency domain. The singularity expansion method (SEM) [60, 61] has been proposed for scattered wave expansion. The time domain electric field scattered by the target is divided into an early-time response and a late-time response. An early time response arises when the excitation wavefront traverses the target and a late time response appears as the excitation wavefront moves beyond the target. As the incident pulse passes across the target, specular reflections are returned from scattering centers, providing an early time response. The late time response of a target can be decomposed into a sum of damped sinusoids oscillating at natural frequencies determined by the geometry of the target [60, 61]. The natural frequencies of a radar target are aspect independent features of its transient electromagnetic response, and there have been many studies on the natural frequency-based radar target recognition [62–64, 67–70].

The authors presented the new formulation of the natural frequency-based radar target recognition scheme based on the least squares estimate in the time domain [62] and frequency domain [63].

The authors presented a numerical scheme for performance

analysis of the natural frequency-based target discrimination scheme in the time domain [64]. It is based on the binary hypothesis testing and a numerical evaluation of a probability density function (PDF). In this paper, we consider the problem in the frequency domain.

The performance analysis of the natural frequency-based radar target recognition in the frequency domain is considered in this paper. The difference between this paper and the previous paper [64] is as follows:

(i) The previous performance analysis [64] is for the time domain. Our scheme is for the frequency domain. While transient late time response is real-valued, the frequency response is complex-valued.

(ii) In the time domain approach presented [64], the zero-mean Gaussian noise with variance of σ^2 is employed. For complex-valued frequency response, it is assumed that the zero-mean Gaussian noise with equal variance is added to the real part of the frequency response and imaginary part of the frequency response, respectively. Without loss of generality, the variance of the zero-mean Gaussian noise for the complex-valued frequency response is set to $\frac{\sigma^2}{2}$.

(iii) In the time domain, the degree-of-freedom of the chi-square distribution is M, which is the number of the natural frequencies considered. In the frequency domain, it is $2M$, not M. The real part and the imaginary part of the frequency response are the zero-mean Gaussian-distributed with variance of $\frac{\sigma^2}{2}$. Therefore, the number of the independent Gaussian random variables is two times the number of the natural frequencies.

(iv) In the time domain, the covariance matrix of the Gaussian random vector is $\sigma^2 \mathbf{I}_{M \times M}$. In the frequency domain, the covariance matrix of the Gaussian random vector is $\frac{\sigma^2}{2} \mathbf{I}_{2M \times 2M}$. $\mathbf{I}_{M \times M}$ and $\mathbf{I}_{2M \times 2M}$ denote $M \times M$ identity matrix and $2M \times 2M$ identity matrix, respectively.

The outline of this paper is as follows:

In Section 1, we review the previous research on the natural frequency-based radar target recognition in the time domain and the frequency domain. In addition, the study on the performance analysis of the natural frequency-based radar target recognition in the time domain is described [64]. Finally, we described how our scheme proposed in this paper is different from the scheme presented in the previous paper [64].

In Section 2, we show how the frequency response of the radar target can be formulated using the natural frequencies.

Performance analysis based on the PDF for two targets is presented in Section 3. Assume that there are two targets of target 1 and target 2. We first define the projection matrix onto the column space of the matrix associated with the natural frequency of the specific target. The difference of the square of the magnitude of the projection of the response of target k onto two matrices is defined where k can be either 1 or 2. Two matrices are defined using the two sets of the natural frequencies of target 1 and target 2. This difference is denoted by $Z_{21|k}$. The characteristic function of $Z_{21|k}$ is derived, and finally the probability density function (PDF) of $Z_{21|k}$ is derived. The probability of the correct classification, given the k-th target, is calculated for both $k = 1$ and $k = 2$. Finally, the average probability of the correct classification is calculated.

In Section 4, performance analysis for two targets presented in Section 3 is extended to the case that there are more than two targets. We derive the upper and lower bounds of the probability of the correct classification.

In Section 5, we present numerical results to validate the derived analytical performance by comparing it with the simulation performance, where it is shown that the simulation performance and the analytical performance show a very good agreement for two targets and that simulation performance is between the upper and lower bounds for more than two targets. Note that the upper and lower bounds are calculated from the analytical approach. In Section 6, we present the conclusions.

2. FORMULATION IN FREQUENCY DOMAIN

It can be easily shown that, based on the late time representation using the natural frequencies, the frequency response can be written as [63], for the k-th target,

$$Y_{n|k} = U_{n|k} + H_{n|k} = \sum_{m=1}^{M_k} \frac{c_{m|k}}{j\omega_n - s_{m|k}} + H_{n|k} \quad n = 1, 2, \ldots, N \quad (1)$$

where N is the number of the sampled frequency response and M_k the number of natural frequencies of the target k.

The real and imaginary parts of $H_{n|k}$ are the zero-mean Gaussian distributed with variance of $\frac{\sigma^2}{2}$, associated with $Y_{n|k}$. $s_{m|k}$, $m = 1, \ldots, M$, is the natural frequencies of the k-th target. $U_{n|k}$, $n = 1, \ldots, N$, is the noiseless frequency response of the k-th target.

If we define

$$\mathbf{Y}_k = \begin{bmatrix} Y_{1|k} & Y_{2|k} & \cdots & Y_{N|k} \end{bmatrix}^{\mathrm{T}} \tag{2}$$

$$\mathbf{c}_k = \begin{bmatrix} c_{1|k} & c_{2|k} & \cdots & c_{M|k} \end{bmatrix}^{\mathrm{T}} \tag{3}$$

$$\mathbf{H}_k = \begin{bmatrix} H_{1|k} & H_{2|k} & \cdots & H_{N|k} \end{bmatrix}^{\mathrm{T}} \tag{4}$$

$$\mathbf{U}_k = \begin{bmatrix} U_{1|k} & U_{2|k} & \cdots & U_{N|k} \end{bmatrix}^{\mathrm{T}}, \tag{5}$$

(1) can be written as

$$\mathbf{Y}_k = \mathbf{B}_k \mathbf{c}_k + \mathbf{H}_k = \mathbf{U}_k + \mathbf{H}_k \tag{6}$$

where $\{\mathbf{B}_k\}_{mn}$ is defined as

$$\{\mathbf{B}_k\}_{mn} = (j\omega_m - s_{n|k})^{-1}. \tag{7}$$

3. PERFORMANCE ANALYSIS FOR TWO TARGETS

Following the discussion in the previous paper [64], we define $Z_{21|k}$ as

$$Z_{21|k} = \|\mathbf{P}_2 \mathbf{Y}_k\|^2 - \|\mathbf{P}_1 \mathbf{Y}_k\|^2 = \mathbf{Y}_k^{\mathrm{H}} \mathbf{P}_2 \mathbf{Y}_k - \mathbf{Y}_k^{\mathrm{H}} \mathbf{P}_1 \mathbf{Y}_k \overset{\text{target 2}}{\underset{\text{target 1}}{\gtrless}} 0 \quad k = 1, 2 \tag{8}$$

where k denotes that the noisy frequency response is from the k-th target and the projection matrices $\mathbf{P}_1$ and $\mathbf{P}_2$ are defined as

$$\mathbf{P}_2 = \mathbf{B}_2 \left(\mathbf{B}_2^{\mathrm{H}} \mathbf{B}_2 \right)^{-1} \mathbf{B}_2^{\mathrm{H}} \tag{9}$$

$$\mathbf{P}_1 = \mathbf{B}_1 \left(\mathbf{B}_1^{\mathrm{H}} \mathbf{B}_1 \right)^{-1} \mathbf{B}_1^{\mathrm{H}}. \tag{10}$$

Note that, in (8), a Hermitian should be used instead of a transpose since $\mathbf{Y}_k$ is a complex random vector.

From the eigen-decomposition of the matrix, $\mathbf{P}_2 - \mathbf{P}_1$, (8) can be written as

$$Z_{21|k} = \mathbf{Y}_k^{\mathrm{H}} \left(\mathbf{P}_2 - \mathbf{P}_1 \right) \mathbf{Y}_k = \mathbf{Y}_k^{\mathrm{H}} \mathbf{V} \Lambda_{21} \mathbf{V}^{\mathrm{H}} \mathbf{Y}_k = \mathbf{W}_k^{\mathrm{H}} \Lambda_{21} \mathbf{W}_k \tag{11}$$

where $\mathbf{W}_k$ is defined from $\mathbf{W}_k = \mathbf{V}^{\mathrm{H}} \mathbf{Y}_k$.

In the case that the number of natural frequencies of the second target, M_2, is greater than the number of natural frequencies of the first target, M_1. The eigenvalues of the matrix, $\mathbf{P}_2 - \mathbf{P}_1$, are given by [98]

$$\Lambda_{21} = \text{diag} \left(\lambda_1, \lambda_2, \ldots, \lambda_{M_2 - M_1}, \ldots, \lambda_{M_2 + M_1}, 0, \ldots, 0 \right) \tag{12}$$

where

$$\lambda_1 = \lambda_2 = \ldots = \lambda_{M_2 - M_1} = 1 \tag{13}$$

$$1 > \lambda_{M_2 - M_1 + 1} > \ldots > \lambda_{M_2 + M_1} > 0. \tag{14}$$

Using (12) in (11), we have

$$Z_{21|k} = F_{21|k} + G_{21|k} \tag{15}$$

$$F_{21|k} = \sum_{\ell=1}^{M_2-M_1} (W_{\ell|k})^*(W_{\ell|k}) = \sum_{\ell=1}^{M_2-M_1} |W_{\ell|k}|^2 \tag{16}$$

$$G_{21|k} = \sum_{\ell=M_2-M_1+1}^{M_2+M_1} \lambda_\ell (W_{\ell|k})^*(W_{\ell|k}) = \sum_{\ell=M_2-M_1+1}^{M_2+M_1} \lambda_\ell |W_{\ell|k}|^2. \tag{17}$$

Note that, in the frequency domain, $F_{21|k}$ and $G_{21|k}$ are defined from the sum of square of $\|W_{l|k}\|$, not the sum of square of $W_{l|k}$. On the other hand, in the time domain [64], $F_{21|k}$ and $G_{21|k}$ are defined from the sum of square of $W_{l|k}$.

Keeping in mind that (13) is true, (15) can also be written as

$$Z_{21|k} = \sum_{p=1}^{M_2+M_1} \lambda_p |W_{p|k}|^2 \tag{18}$$

$$= \sum_{p=1}^{M_2+M_1} \lambda_p \left\{ (\mathrm{Re}(W_{p|k}))^2 + (\mathrm{Im}(W_{p|k}))^2 \right\} \tag{19}$$

$$\lambda_1 = \lambda_2 = \ldots = \lambda_{M_2-M_1} = 1. \tag{20}$$

We list some identities used for further derivation:

$$\mu_{\mathrm{Re}(W_{p|k})} \equiv E\left[\mathrm{Re}\left(W_{p|k}\right)\right] = \mathrm{Re}\left[E\left(W_{p|k}\right)\right] \equiv \mathrm{Re}\left(\mu_{W_{p|k}}\right) \tag{21}$$

$$\mu_{\mathrm{Im}(W_{p|k})} \equiv E\left[\mathrm{Im}\left(W_{p|k}\right)\right] = \mathrm{Im}\left[E\left(W_{p|k}\right)\right] \equiv \mathrm{Im}\left(\mu_{W_{p|k}}\right) \tag{22}$$

$$E\left[(\mathrm{Re}(W_{p|k}))^2\right] = \left[E\left(\mathrm{Re}(W_{p|k})\right)\right]^2 + \mathrm{var}\left(\mathrm{Re}(W_{p|k})\right) \tag{23}$$

$$E\left[(\mathrm{Im}(W_{p|k}))^2\right] = \left[E\left(\mathrm{Im}(W_{p|k})\right)\right]^2 + \mathrm{var}\left(\mathrm{Im}(W_{p|k})\right) \tag{24}$$

$$E\left(|W_{p|k}|^2\right) = E\left((\mathrm{Re}(W_{p|k}))^2 + (\mathrm{Im}(W_{p|k}))^2\right)$$

$$= E\left((\mathrm{Re}(W_{p|k}))^2\right) + E\left((\mathrm{Im}(W_{p|k}))^2\right) \tag{25}$$

$$E\left[(\mathrm{Re}\left(W_{p|k}\right))^4\right] = \left[E\left(\mathrm{Re}\left(W_{p|k}\right)\right)\right]^4 + 6\left[E\left(\mathrm{Re}\left(W_{p|k}\right)\right)\right]^2$$

$$\left(\mathrm{var}\left(\mathrm{Re}\left(W_{p|k}\right)\right)\right) + 3\left(\mathrm{var}\left(\mathrm{Re}\left(W_{p|k}\right)\right)\right)^2 \tag{26}$$

$$E\left[(\mathrm{Im}\left(W_{p|k}\right))^4\right] = \left[E\left(\mathrm{Im}\left(W_{p|k}\right)\right)\right]^4 + 6\left[E\left(\mathrm{Im}\left(W_{p|k}\right)\right)\right]^2$$

$$\left(\mathrm{var}\left(\mathrm{Im}\left(W_{p|k}\right)\right)\right) + 3\left(\mathrm{var}\left(\mathrm{Im}\left(W_{p|k}\right)\right)\right)^2. \tag{27}$$

$\text{Re}(Y_{p|k})$ and $\text{Im}(Y_{p|k})$ are Gaussian distributed with variance of $\frac{\sigma^2}{2}$. $\mathbf{W}$ is defined from $\mathbf{W} = \mathbf{V}^H \mathbf{Y}$ where $\mathbf{V}$ is an unitary matrix. Therefore, $\text{Re}(W_{p|k})$ and $\text{Im}(W_{p|k})$ are also Gaussian-distributed with variance of $\frac{\sigma^2}{2}$.

Using (21)–(27) in (19), the mean of $Z_{21|k}$, assuming that the k-th target is present, is given by

$$
\begin{aligned}
\mu_{Z_{21|k}} &= \sum_{p=1}^{M_2+M_1} \lambda_p \left(\frac{\sigma^2}{2} + \left(\mu_{\text{Re}(W_{p|k})} \right)^2 + \frac{\sigma^2}{2} + \left(\mu_{\text{Im}(W_{p|k})} \right)^2 \right) \\
&= \sum_{p=1}^{M_2+M_1} \lambda_p \left(\sigma^2 + \left| \mu_{W_{p|k}} \right|^2 \right).
\end{aligned}
\tag{28}
$$

From (18), we have

$$
\begin{aligned}
\left(Z_{21|k} \right)^2 &= \left(\lambda_1 \left| W_{1|k} \right|^2 + \ldots + \lambda_{M_2+M_1} \left| W_{M_2+M_1|k} \right|^2 \right)^2 \\
&= \sum_{p=1}^{M_2+M_1} \lambda_p^2 \left| W_{p|k} \right|^4 + 2 \sum_{p=1}^{M_2+M_1-1} \sum_{q=p+1}^{M_2+M_1} \lambda_p \lambda_q \left| W_{p|k} \right|^2 \left| W_{q|k} \right|^2 \\
&= \sum_{p=1}^{M_2+M_1} \lambda_p^2 \left[\left(\text{Re}(W_{p|k})^2 \right)^4 + \left(\text{Im}(W_{p|k})^2 \right)^4 \right. \\
&\quad \left. + 2 \left(\text{Re}(W_{p|k}) \right)^2 \left(\text{Im}(W_{p|k}) \right)^2 \right] \\
&\quad + 2 \sum_{p=1}^{M_2+M_1-1} \left[\sum_{q=p+1}^{M_2+M_1} \lambda_p \lambda_q \left\{ \left(\text{Re}(W_{p|k}) \right)^2 + \left(\text{Im}(W_{p|k}) \right)^2 \right\} \right. \\
&\quad \left. \times \left\{ \left(\text{Re}(W_{q|k}) \right)^2 + \left(\text{Im}(W_{q|k}) \right)^2 \right\} \right].
\end{aligned}
\tag{29}
$$

Using (21)–(27) in (29), $E((Z_{21|k})^2)$ are given by

$$
\begin{aligned}
E\left((Z_{21|k})^2 \right) &= \sum_{p=1}^{M_2+M_1} \lambda_p^2 \left\{ \left(\mu_{\text{Re}(W_{p|k})} \right)^4 + 6 \left(\mu_{\text{Re}(W_{p|k})} \right)^2 \frac{\sigma^2}{2} + 3 \frac{\sigma^4}{4} \right. \\
&\quad + \left(\mu_{\text{Im}(W_{p|k})} \right)^4 + 6 \left(\mu_{\text{Im}(W_{p|k})} \right)^2 \frac{\sigma^2}{2} + 3 \frac{\sigma^4}{4} \\
&\quad \left. + 2 \left(\frac{\sigma^2}{2} + \left(\mu_{\text{Re}(W_{p|k})} \right)^2 \right) \left(\frac{\sigma^2}{2} + \left(\mu_{\text{Im}(W_{p|k})} \right)^2 \right) \right\} \\
&\quad + \sum_{p=1}^{M_2+M_1-1} \left[\sum_{q=p+1}^{M_2+M_1} \lambda_p \lambda_q \left(\sigma^2 + \left| \mu_{W_{p|k}} \right|^2 \right) \right.
\end{aligned}
$$

$$\times \left(\sigma^2 + \left| \mu_{W_{q|k}} \right|^2 \right) \Bigg]. \tag{30}$$

From (28) and (30), $\sigma_{Z_{21|k}}^2$ can be given by

$$\sigma_{Z_{21|k}}^2 = \sum_{p=1}^{M_2+M_1} \lambda_p^2 \left(\left(\mu_{\mathrm{Re}(W_{p|k})} \right)^4 + \left(\mu_{\mathrm{Im}(W_{p|k})} \right)^4 + 4\sigma^2 \left| \mu_{W_{p|k}} \right|^2 \right.$$

$$+ 2\sigma^4 + 2 \left(\mu_{\mathrm{Re}(W_{p|k})} \right)^2 \left(\mu_{\mathrm{Im}(W_{p|k})} \right)^2 \right)$$

$$+ 2 \sum_{p=1}^{M_2+M_1-1} \left[\sum_{q=p+1}^{M_2+M_1} \lambda_p \lambda_q \left(\sigma^2 + \left| \mu_{W_{p|k}} \right|^2 \right) \right.$$

$$\times \left(\sigma^2 + \left| \mu_{W_{q|k}} \right|^2 \right) \Bigg] - \left(\mu_{Z_{21|k}} \right)^2$$

$$= \sum_{p=1}^{M_2+M_1} \lambda_p^2 \left(\left| \mu_{W_{p|k}} \right|^4 + 4\sigma^2 \left| \mu_{W_{p|k}} \right|^2 + 2\sigma^4 \right)$$

$$+ 2 \sum_{p=1}^{M_2+M_1-1} \left\{ \sum_{q=p+1}^{M_2+M_1} \lambda_p \lambda_q \right.$$

$$\times \left(\sigma^2 + \left| \mu_{W_{p|k}} \right|^2 \right) \left(\sigma^2 + \left| \mu_{W_{q|k}} \right|^2 \right) \right\} - \left(\mu_{Z_{21|k}} \right)^2. \tag{31}$$

In order to get the PDF from the inverse Fourier-transform [23, 96, 97] of characteristic function, the characteristic function should be sampled at discrete angular frequencies. The sampling interval $\omega_{s|k}$ is

$$\omega_{s|k} = \frac{\pi}{\zeta_k} \tag{32}$$

where ζ_k is the limit above which the value of the PDF can be practically set to be zero [5].

$$\zeta_k = \begin{cases} \zeta_k = \mu_{Z_{21|k}} + 6\sigma_{Z_{21|k}}, & \mu_{Z_{21|k}} > 0 \\ \zeta_k = -\left(\mu_{Z_{21|k}} - 6\sigma_{Z_{21|k}} \right), & \mu_{Z_{21|k}} < 0 \end{cases} \tag{33}$$

Note that $\mu_{Z_{21|k}}$ and $\sigma_{Z_{21|k}}$ can be calculated from (28) and (31), respectively.

To get an analytic expression of the characteristic function of $F_{21|k}$, we rewrite $F_{21|k}$ as

$$F_{21|k} = \sum_{\ell=1}^{M_2-M_1} \left| W_{\ell|k} \right|^2 = \sum_{\ell=1}^{M_2-M_1} \left[\left(\mathrm{Re}\left(W_{\ell|k} \right) \right)^2 + \left(\mathrm{Im}\left(W_{\ell|k} \right) \right)^2 \right]. \tag{34}$$

We define $F_{21,R|k}$ and $F_{21,I|k}$ as

$$F_{21,R|k} \equiv \sum_{\ell=1}^{M_2-M_1} \left(\mathrm{Re}(W_{\ell|k})\right)^2 \qquad (35)$$

$$F_{21,I|k} \equiv \sum_{\ell=1}^{M_2-M_1} \left(\mathrm{Im}(W_{\ell|k})\right)^2. \qquad (36)$$

The characteristic functions of $F_{21,R|k}$ and $F_{21,I|k}$ can be expressed as

$$\Phi_{F_{21,R|k}}(j\omega) = \frac{1}{\left(1-j2\omega\frac{\sigma^2}{2}\right)^{\frac{M_2-M_1}{2}}} \exp\left(\frac{j\omega \sum_{p=1}^{M_2-M_1} \left(\mu_{\mathrm{Re}(W_{p|k})}\right)^2}{\left(1-j2\omega\frac{\sigma^2}{2}\right)}\right) \qquad (37)$$

$$\Phi_{F_{21,I|k}}(j\omega) = \frac{1}{\left(1-j2\omega\frac{\sigma^2}{2}\right)^{\frac{M_2-M_1}{2}}} \exp\left(\frac{j\omega \sum_{p=1}^{M_2-M_1} \left(\mu_{\mathrm{Im}(W_{p|k})}\right)^2}{\left(1-j2\omega\frac{\sigma^2}{2}\right)}\right). \qquad (38)$$

Since $F_{21|k} = F_{21,R|k} + F_{21,I|k}$, we have

$$\Phi_{F_{21|k}}(j\omega) = \Phi_{F_{21,R|k}}(j\omega) \times \Phi_{F_{21,I|k}}(j\omega)$$

$$= \frac{1}{(1-j\omega\sigma^2)^{M_2-M_1}} \exp\left(\frac{j\omega \sum_{p=1}^{M_2-M_1} \left|\mu_{W_{p|k}}\right|^2}{(1-j\omega\sigma^2)}\right). \qquad (39)$$

$G_{21|k}$ can be written as

$$G_{21|k} = \sum_{\ell=M_2-M_1+1}^{M_2+M_1} \lambda_\ell \left|W_{\ell|k}\right|^2$$

$$= \sum_{\ell=M_2-M_1+1}^{M_2+M_1} \lambda_\ell \left[\left(\mathrm{Re}\left(W_{\ell|k}\right)\right)^2 + \left(\mathrm{Im}\left(W_{\ell|k}\right)\right)^2\right]. \qquad (40)$$

Similarly, $G_{21,R|k}$ and $G_{21,I|k}$ are defined as

$$G_{21,R|k} \equiv \sum_{\ell=M_2-M_1+1}^{M_2+M_1} \lambda_\ell \left(\mathrm{Re}(W_{\ell|k})\right)^2 \qquad (41)$$

$$G_{21,I|k} \equiv \sum_{\ell=M_2-M_1+1}^{M_2+M_1} \lambda_\ell \left(\mathrm{Im}(W_{\ell|k})\right)^2. \qquad (42)$$

The corresponding characteristic functions are

$$\Phi_{G_{21,R|k}}(j\omega)$$

$$= \prod_{p=M_2-M_1+1}^{M_2+M_1} \left[\frac{\lambda_p}{|\lambda_p| \left(1-j2\omega\lambda_p\frac{\sigma^2}{2}\right)^{0.5}} \times \exp\left(\frac{j\omega\left(\mu_{\mathrm{Re}(W_{p|k})}\right)^2\lambda_p}{\left(1-j2\omega\lambda_p\frac{\sigma^2}{2}\right)} \right) \right] \quad (43)$$

$$\Phi_{G_{21,I|k}}(j\omega)$$

$$= \prod_{p=M_2-M_1+1}^{M_2+M_1} \left[\frac{\lambda_p}{|\lambda_p| \left(1-j2\omega\lambda_p\frac{\sigma^2}{2}\right)^{0.5}} \times \exp\left(\frac{j\omega\left(\mu_{\mathrm{Im}(W_{p|k})}\right)^2\lambda_p}{\left(1-j2\omega\lambda_p\frac{\sigma^2}{2}\right)} \right) \right]. \quad (44)$$

The characteristic function of $G_{21|k}$ is

$$\Phi_{G_{21|k}}(j\omega) = \Phi_{G_{21,R|k}}(j\omega) \times \Phi_{G_{21,I|k}}(j\omega)$$

$$= \prod_{p=M_2-M_1+1}^{M_2+M_1} \frac{1}{(1-j\omega\lambda_p\sigma^2)} \exp\left(\frac{j\omega\left|\mu_{W_{p|k}}\right|^2\lambda_p}{(1-j\omega\lambda_p\sigma^2)} \right). \quad (45)$$

Finally, using (39) and (45), the characteristic function of $Z_{21|k}$ is

$$\Phi_{Z_{21|k}}(j\omega) = \Phi_{F_{21|k}}(j\omega) \times \Phi_{G_{21|k}}(j\omega). \quad (46)$$

Using the inverse Fourier transform, the PDF of $Z_{21|k}$ is given by

$$p_{Z_{21|k}} = \mathrm{IFFT}\left(\Phi_{Z_{21|k}}(j\omega) \right). \quad (47)$$

The procedure for getting the PDF $p_{Z_{21|k}}$ can be summarized as

(i) Determine the average noise variance of $\frac{\sigma^2}{2}$ of the real part and the imaginary part of $H_{n|k}$ in (1).

(ii) Get the eigenvectors and the eigenvalues of the matrix $\mathbf{P}_2 - \mathbf{P}_1$ where $\mathbf{P}_2$ and $\mathbf{P}_1$ are given in (9) and (10), respectively.

(iii) $\mathbf{U}_k$ denotes the noiseless frequency response from the k-th target in (5).

(iv) Compute the mean vector of $\mathbf{W}_k = \mathbf{V}^{\mathrm{H}}\mathbf{Y}_k$, which is given by $\mu_{\mathbf{W}_k} = \mathbf{V}^{\mathrm{H}}\mathbf{U}_k$.

(v) Calculate $\mu_{Z_{21|k}}$ and $\sigma^2_{Z_{21|k}}$ using (28) and (31), respectively.

(vi) Determine $\omega_{s|k}$ of the characteristic function using (32) and (33).

(vii) Calculate $\Phi_{F_{21,R|k}}(j\omega)$ using (37) at integer multiples of $\omega_{s|k}$.

(viii) Determine $\Phi_{F_{21,I|k}}(j\omega)$ using (38) at integer multiples of $\omega_{s|k}$.

(ix) Determine $\Phi_{F_{21|k}}(j\omega)$ using (39) at integer multiples of $\omega_{s|k}$.

(x) Calculate $\Phi_{G_{21,R|k}}(j\omega)$ using (43) at integer multiples of $\omega_{s|k}$.

(xi) Determine $\Phi_{G_{21,I|k}}(j\omega)$ using (44) at integer multiples of $\omega_{s|k}$.

(xii) Determine $\Phi_{G_{21|k}}(j\omega)$ using (45) at integer multiples of $\omega_{s|k}$.

(xiii) Evaluate $\Phi_{Z_{21|k}}(j\omega)$ using (46) at integer multiples of $\omega_{s|k}$.

(xiv) Evaluate $p_{Z_{21|k}}$ using (47).

So far, we assume that M_2 is greater than M_1. For $M_1 > M_2$, we define

$$Z_{12} = \mathbf{Y}^{\mathrm{H}}\left(\mathbf{P}_1 - \mathbf{P}_2\right)\mathbf{Y}. \tag{48}$$

In that case, the eigenvalues of the matrix $\mathbf{P}_1 - \mathbf{P}_2$ are given by

$$\Lambda_{12} = \mathrm{diag}\left(\lambda_1, \ldots, \lambda_{M_1-M_2}, -\lambda_{M_1-M_2+1} \ldots, -\lambda_{M_2+M_1}, 0, \ldots, 0\right) \tag{49}$$

where

$$\lambda_1 = \lambda_2 = \ldots = \lambda_{M_2-M_1} = -1. \tag{50}$$

We can use the fact the PDF of $Z_{12|k}$ is related to that of $Z_{21|k}$ as follows:

$$p_{Z_{21|k}}(z) = p_{Z_{12|k}}(-z) \tag{51}$$

The probability of the correct classification is obtained from the PDF as follows:

$$P_{I|2} = \mathrm{Prob}(Z_{21|k} > 0\,|k=2) = \int_0^\infty p_{Z_{21|2}}(z)dz \tag{52}$$

$$P_{I|1} = \mathrm{Prob}(Z_{21|k} < 0\,|k=1) = \int_{-\infty}^0 p_{Z_{21|1}}(z)dz \tag{53}$$

$$P_I = \sum_{m=1}^2 P_{I|m}\,\mathrm{Prob}(m\text{-th target is present}) = \frac{1}{2}\sum_{m=1}^2 P_{I|m} \tag{54}$$

where $P_{I|2}$ is the probability of the correct classification given that the second target is present and $P_{I|1}$ is the probability of the correct classification given that the first target is present.

4. PERFORMANCE ANALYSIS FOR MULTIPLE TARGETS

Assuming that the k-th target is present, the probability of the correct classification can be written as

$$\begin{aligned}
P_{I|k} = \mathrm{Prob}\Big[&\mathbf{Y}^{\mathrm{H}}\mathbf{P}_k\mathbf{Y} > \mathbf{Y}^{\mathrm{H}}\mathbf{P}_1\mathbf{Y}, \ldots, \mathbf{Y}^{\mathrm{H}}\mathbf{P}_k\mathbf{Y} > \\
&\mathbf{Y}^{\mathrm{H}}\mathbf{P}_{k-1}\mathbf{Y}, \ldots, \mathbf{Y}^{\mathrm{H}}\mathbf{P}_k\mathbf{Y} > \mathbf{Y}^{\mathrm{H}}\mathbf{P}_{k+1}\mathbf{Y}, \ldots, \mathbf{Y}^{\mathrm{H}}\mathbf{P}_k\mathbf{Y} \\
&> \mathbf{Y}^{\mathrm{H}}\mathbf{P}_M\mathbf{Y}\,|k\text{th target}\Big].
\end{aligned} \tag{55}$$

Since evaluating (55) is quite challenging, we try to get the upper and lower bounds of the probability of the correct classification.

Assuming that the correct target is the k-th target, the upper and lower bounds of the correct classification are given by [5]

$$P_{I|k}^{\mathrm{up}} = \min_{i \neq k} \left\{ \int_0^\infty p_{Z_{ki|k}}(z)dz \right\} \tag{56}$$

$$P_{I|k}^{\mathrm{lo}} = \max \left\{ 0, 1 - \sum_{\substack{i=1 \\ i \neq k}}^{M} \int_{-\infty}^0 p_{Z_{ki|k}}(z)dz \right\}. \tag{57}$$

Note that the PDF's in (56) and (57) are evaluated using the scheme in Section 3.

The upper and lower bounds of the correct classification, considering all M targets, are given by

$$P_I^{\mathrm{up}} = \frac{1}{M} \sum_{m=1}^{M} P_{I|m}^{\mathrm{up}} \tag{58}$$

$$P_I^{\mathrm{lo}} = \frac{1}{M} \sum_{m=1}^{M} P_{I|m}^{\mathrm{lo}}. \tag{59}$$

5. NUMERICAL RESULTS

When we only consider two targets, we compare the analytic results in (54) with the simulation-based performance. For multiple targets, the analytic results in (59) and (58) are compared with the results based on the Monte-Carlo simulation. In getting the simulation-based performance, the probability of correct classification is obtained from 10,000 repetitions.

The noiseless frequency response is obtained via the method of moments (MoM). We calculated the back-scattered field. The frequency response up to 0.5 GHz is obtained in increments of 7.8 MHz. The incident angles for all the numerical examples are $\theta = [20° \ 40° \ 60° \ 80°]$.

The targets for the results in Fig. 1 are two straight wires of length 0.8 meter and 1.4 meter with $\frac{\mathrm{length}}{\mathrm{radius}} = 200$. The natural frequencies for two targets can be found in [5], where we can see that, for the frequency response up to 0.5 GHz, the number of natural frequencies for 0.8 meter-long wire and for 1.4 meter-long wire are $M_1 = 4$ and $M_2 = 8$, respectively. It is illustrated that the analytic performance obtained using (54) shows a good agreement with the performance using the

Monte-Carlo simulation. The results are also tabulated in Table 1 to clearly show the agreement between the numerical performance and the analytical performance.

The natural frequencies for two targets can be found in [64], where we can see that, for the frequency response up to 0.5 GHz, the number of the natural frequencies for 0.8 meter-long wire and for 1.4 meter-long wire are $M_1 = 4$ and $M_2 = 8$, respectively. It is illustrated that the analytic performance obtained using (54) shows a good agreement with the performance using the Monte-Carlo simulation. The results are also tabulated in Table 1 to clearly show the agreement between the numerical performance and the analytical performance.

Three straight wires of length 0.7 meter, 1 meter and 1.3 meter with $\frac{length}{radius} = 200$ are used for the results in Fig. 2. For the frequency response up to 0.5 GHz, M_1, M_2 and M_3 are 4, 6 and 8, respectively [64]. From Fig. 2 and Table 2, we can clearly see that the simulation performance is between the upper and lower bounds, where the upper and lower bounds are analytical derived.

In Fig. 3, we consider four straight wires with different lengths of

Table 1. Analytic performance and simulated performance for two straight wires (numerical values).

$\theta = 20°$, $M_1 = 4$, $M_2 = 8$									
SNR	−20	−15	−10	−5	0	5	10	15	20
Simulation	0.5	0.5	0.53	0.61	0.82	0.98	1	1	1
Analytic	0.5	0.51	0.54	0.63	0.84	0.98	1	1	1
$\theta = 40°$, $M_1 = 4$, $M_2 = 8$									
SNR	−20	−15	−10	−5	0	5	10	15	20
Simulation	0.5	0.5	0.53	0.63	0.84	0.99	1	1	1
Analytic	0.5	0.51	0.54	0.64	0.86	0.99	1	1	1
$\theta = 60°$, $M_1 = 4$, $M_2 = 8$									
SNR	−20	−15	−10	−5	0	5	10	15	20
Simulation	0.5	0.51	0.53	0.64	0.87	0.99	1	1	1
Analytic	0.5	0.51	0.54	0.66	0.89	0.99	1	1	1
$\theta = 80°$, $M_1 = 4$, $M_2 = 8$									
SNR	−20	−15	−10	−5	0	5	10	15	20
Simulation	0.5	0.5	0.53	0.61	0.84	0.99	1	1	1
Analytic	0.5	0.51	0.54	0.63	0.86	0.99	1	1	1

0.7 meter, 1.0 meter, 1.3 meter and 1.6 meter. The natural frequencies for the frequency response for the targets can be found in [64], and the numbers of the natural frequencies for all the targets up to 0.5 GHz are $M_1 = 4$, $M_2 = 6$, $M_3 = 8$ and $M_4 = 10$. It is illustrated that the lower and upper bounds obtained from (58) and (59) show a good agreement with the performance using the Monte-Carlo simulation.
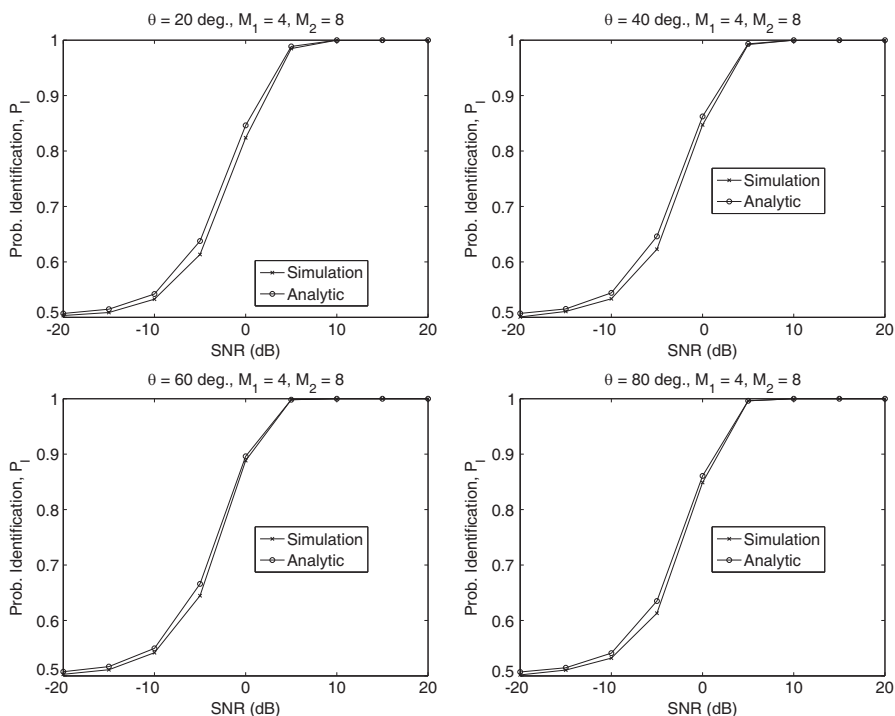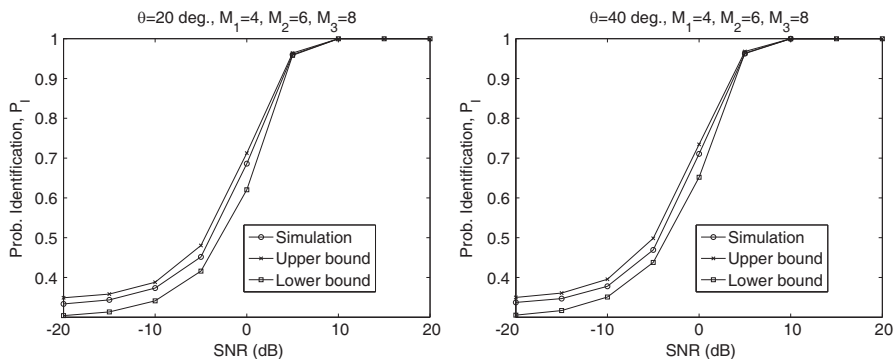
Figure 1. Analytic performance and simulated performance for two straight wires.
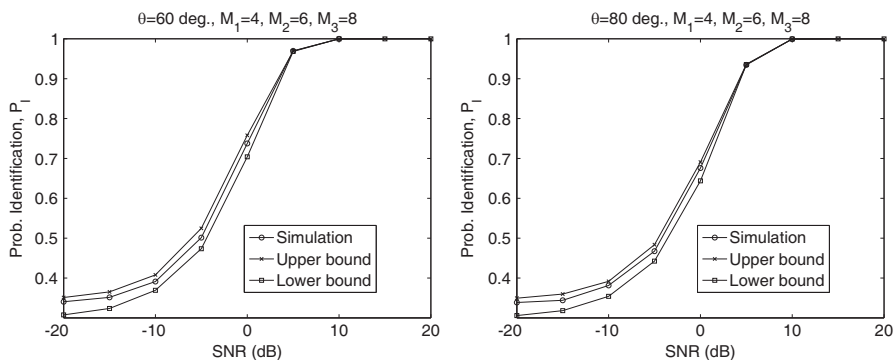
Figure 2. Analytic performance and simulated performance for three straight wires.

Table 2. Analytic performance and simulated performance for three straight wires (numerical values).

| $\theta = 20°$, $M_1 = 4$, $M_2 = 6$, $M_3 = 8$									
SNR	-20	-15	-10	-5	0	5	10	15	20
Simulation	0.33	0.34	0.37	0.45	0.68	0.96	1	1	1
Upper bound	0.34	0.35	0.38	0.48	0.71	0.96	1	1	1
Lower bound	0.3	0.31	0.34	0.41	0.62	0.95	1	1	1
$\theta = 40°$, $M_1 = 4$, $M_2 = 6$, $M_3 = 8$									
SNR	-20	-15	-10	-5	0	5	10	15	20
Simulation	0.33	0.34	0.37	0.46	0.71	0.96	0.99	1	1
Upper bound	0.34	0.36	0.39	0.49	0.73	0.96	1	1	1
Lower bound	0.3	0.31	0.35	0.43	0.65	0.96	1	1	1
$\theta = 60°$, $M_1 = 4$, $M_2 = 6$, $M_3 = 8$									
SNR	-20	-15	-10	-5	0	5	10	15	20
Simulation	0.34	0.35	0.39	0.5	0.73	0.96	0.99	1	1
Upper bound	0.35	0.36	0.4	0.52	0.75	0.96	1	1	1
Lower bound	0.3	0.32	0.36	0.47	0.7	0.96	1	1	1
$\theta = 80°$, $M_1 = 4$, $M_2 = 6$, $M_3 = 8$									
SNR	-20	-15	-10	-5	0	5	10	15	20
Simulation	0.33	0.34	0.38	0.46	0.67	0.93	0.99	1	1
Upper bound	0.34	0.35	0.39	0.48	0.69	0.93	0.99	1	1
Lower bound	0.3	0.31	0.35	0.44	0.64	0.93	0.99	1	1
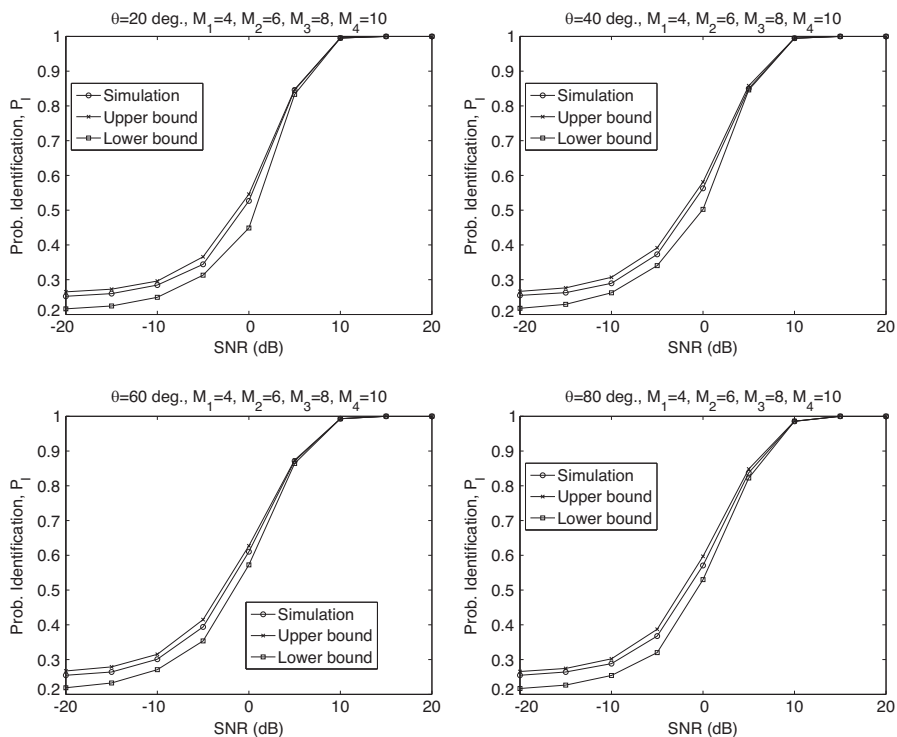
Figure 3. Analytic performance and simulated performance for four straight wires.
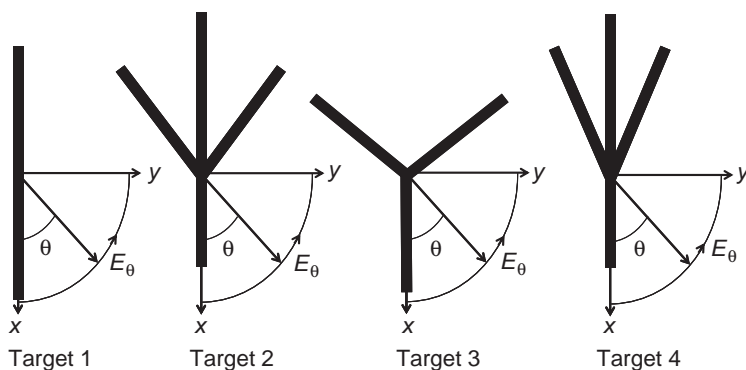

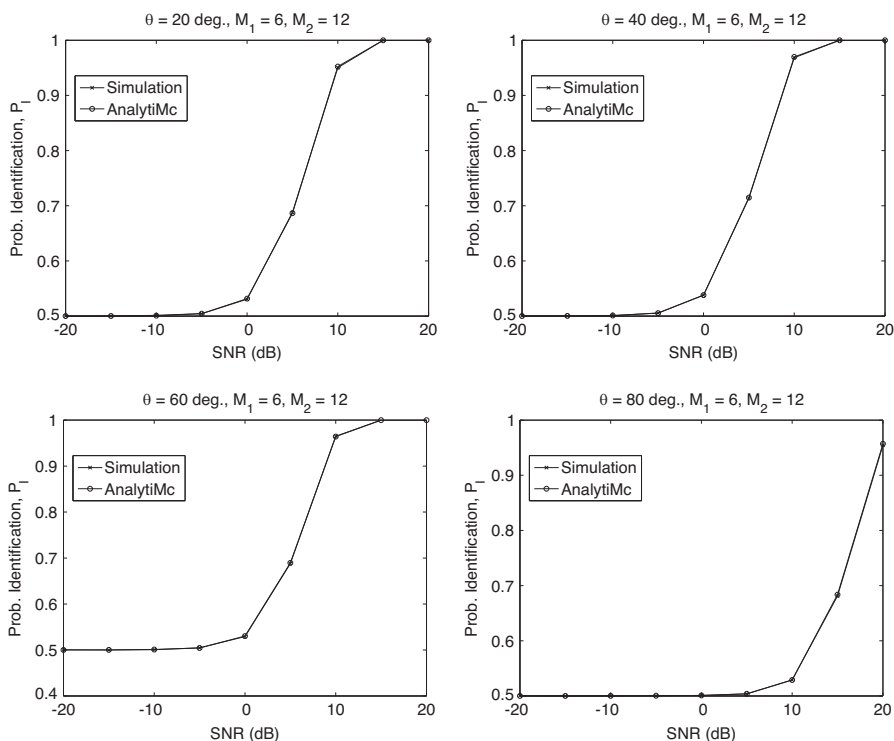**Figure 4.** Four targets used for the results in Figs. 5–7.

Figure 5. Analytic performance and simulated performance for target 1 and target 2 in Fig. 4.

The numerical values of the results in Fig. 3 are tabulated in Table 3, from which it is clear that the simulation performance is actually between the lower and upper bounds of the analytical performance.

In Fig. 4, we illustrate four types of targets used for the results in Figs. 5–7. For more information on the geometric shape and the corresponding natural frequencies for each target, refer to [64]. The radii for all the targets are equal to 0.5 cm.

In the fourth example, we consider target 1 and target 2 in Fig. 4 with $M_1 = 6$, $M_2 = 12$ for frequency response up to 0.5 GHz. The results in Fig. 5 show that the analytic result in (54) can predict the performance by the Monte Carlo simulation obtained from 10,000 repetitions. The numerical values of the results in Fig. 5 are shown in Table 4, where it is shown that the agreement between the analytical and simulated performances is quite excellent.

We consider target 1, target 2 and target 3 in Fig. 4 with $M_1 = 6$, $M_2 = 12$ and $M_3 = 10$ for frequency response up to 0.5 GHz in the fifth

example. The results in Table 5 show the analytic results in Fig. 6. From Table 5 and Fig. 6, it is clear that the simulation performance actually lies between the upper and lower bounds. Note that the upper and lower bounds are obtained from the analytical approach.

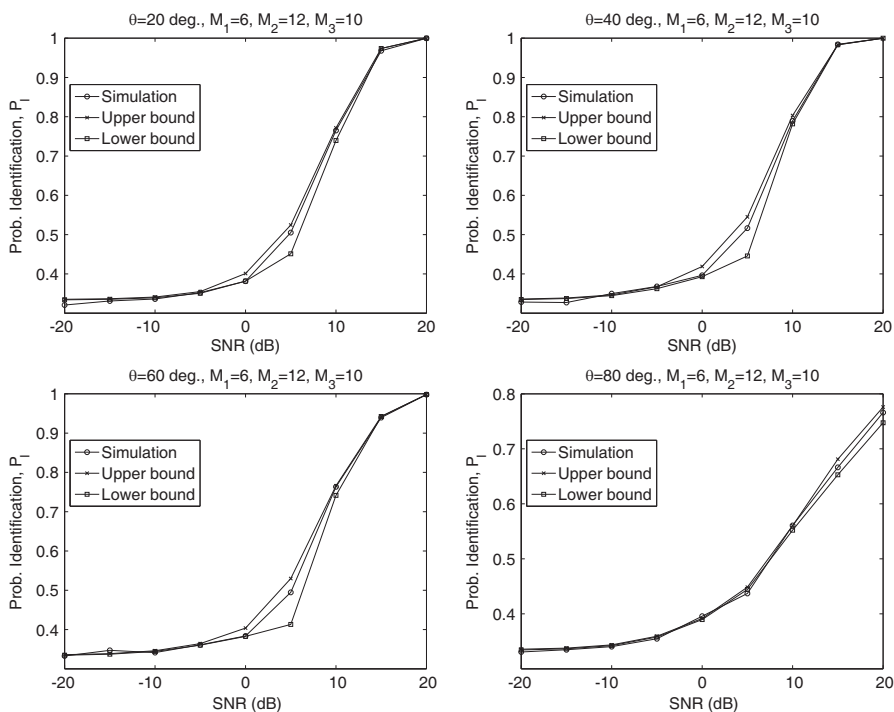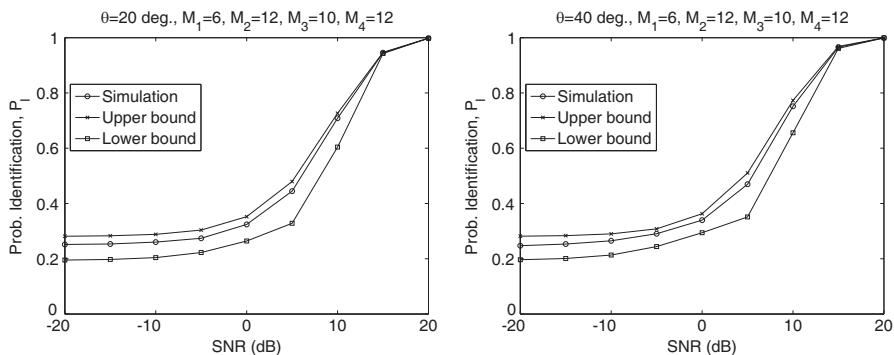The results in Fig. 7 and Table 6 are for the four targets in Fig. 4

Figure 6. Analytic performance and simulated performance for target 1 , target 2 and target 3 in Fig. 4.
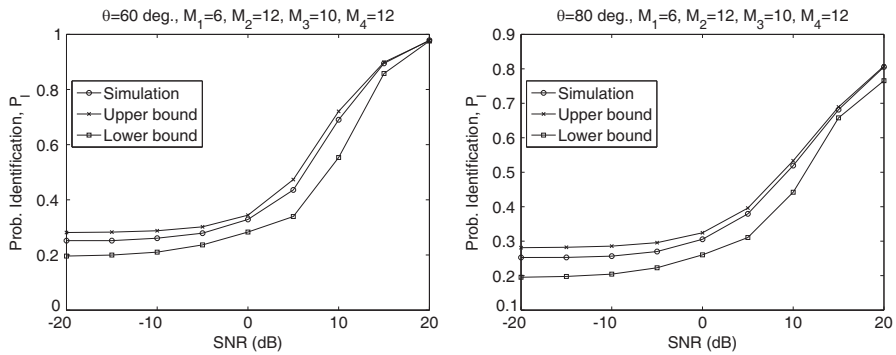
Figure 7. Analytic performance and simulated performance for all the targets in Fig. 4.

Table 3. Analytic performance and simulated performance for four straight wires (numerical values).

$\theta = 20°$, $M_1 = 4$, $M_2 = 6$, $M_3 = 8$, $M_4 = 10$									
SNR	-20	-15	-10	-5	0	5	10	15	20
Simulation	0.25	0.25	0.27	0.34	0.52	0.84	0.99	1	1
Upper bound	0.26	0.27	0.29	0.36	0.54	0.84	0.99	1	1
Lower bound	0.21	0.22	0.24	0.31	0.44	0.83	0.99	1	1
$\theta = 40°$, $M_1 = 4$, $M_2 = 6$, $M_3 = 8$, $M_4 = 10$									
SNR	-20	-15	-10	-5	0	5	10	15	20
Simulation	0.25	0.26	0.29	0.37	0.55	0.85	0.99	1	1
Upper bound	0.26	0.27	0.3	0.39	0.58	0.85	0.99	1	1
Lower bound	0.21	0.22	0.26	0.34	0.5	0.84	0.99	1	1
$\theta = 60°$, $M_1 = 4$, $M_2 = 6$, $M_3 = 8$, $M_4 = 10$									
SNR	-20	-15	-10	-5	0	5	10	15	20
Simulation	0.25	0.26	0.29	0.39	0.6	0.87	0.99	1	1
Upper bound	0.26	0.27	0.31	0.41	0.62	0.87	0.99	1	1
Lower bound	0.21	0.23	0.27	0.35	0.57	0.86	0.99	1	1
$\theta = 80°$, $M_1 = 4$, $M_2 = 6$, $M_3 = 8$, $M_4 = 10$									
SNR	-20	-15	-10	-5	0	5	10	15	20
Simulation	0.25	0.26	0.28	0.36	0.56	0.83	0.98	1	1
Upper bound	0.26	0.27	0.3	0.38	0.59	0.84	0.98	1	1
Lower bound	0.21	0.22	0.25	0.32	0.53	0.82	0.98	1	1

Table 4. Analytic performance and simulated performance for target 1 and target 2 in Fig. 4 (numerical values).

$\theta = 20°$, $M_1 = 6$, $M_2 = 12$									
SNR	-20	-15	-10	-5	0	5	10	15	20
Simulation	0.5	0.5	0.5	0.5	0.53	0.68	0.95	1	1
Analytic	0.5	0.5	0.5	0.5	0.53	0.68	0.95	1	1
$\theta = 40°$, $M_1 = 6$, $M_2 = 12$									
SNR	-20	-15	-10	-5	0	5	10	15	20
Simulation	0.5	0.5	0.5	0.5	0.53	0.71	0.96	1	1
Analytic	0.5	0.5	0.5	0.5	0.53	0.71	0.96	1	1
$\theta = 60°$, $M_1 = 6$, $M_2 = 12$									
SNR	-20	-15	-10	-5	0	5	10	15	20
Simulation	0.5	0.5	0.5	0.5	0.52	0.68	0.96	1	1
Analytic	0.5	0.5	0.5	0.5	0.53	0.68	0.96	1	1
$\theta = 80°$, $M_1 = 6$, $M_2 = 12$									
SNR	-20	-15	-10	-5	0	5	10	15	20
Simulation	0.5	0.5	0.5	0.5	0.5	0.5	0.53	0.68	0.95
Analytic	0.5	0.5	0.5	0.5	0.5	0.5	0.52	0.68	0.95

Table 5. Analytic performance and simulated performance for target 1, target 2 and target 3 in Fig. 4 (numerical values).

$\theta = 20°$, $M_1 = 6$, $M_2 = 12$, $M_3 = 10$									
SNR	-20	-15	-10	-5	0	5	10	15	20
Simulation	0.32	0.33	0.33	0.35	0.38	0.5	0.76	0.96	0.99
Upper bound	0.33	0.33	0.34	0.35	0.4	0.52	0.77	0.97	0.99
Lower bound	0.33	0.33	0.33	0.35	0.38	0.45	0.73	0.97	0.99
$\theta = 40°$, $M_1 = 6$, $M_2 = 12$, $M_3 = 10$									
SNR	-20	-15	-10	-5	0	5	10	15	20
Simulation	0.32	0.32	0.34	0.36	0.39	0.51	0.78	0.98	1
Upper bound	0.33	0.33	0.34	0.36	0.41	0.54	0.8	0.98	1
Lower bound	0.33	0.33	0.34	0.36	0.39	0.44	0.78	0.98	1
$\theta = 60°$, $M_1 = 6$, $M_2 = 12$, $M_3 = 10$									
SNR	-20	-15	-10	-5	0	5	10	15	20
Simulation	0.33	0.34	0.34	0.36	0.38	0.49	0.76	0.93	0.99
Upper bound	0.33	0.33	0.34	0.36	0.4	0.52	0.76	0.94	0.99

Lower bound	0.33	0.33	0.34	0.36	0.38	0.41	0.74	0.94	0.99
$\theta = 80°$, $M_1 = 6$, $M_2 = 12$, $M_3 = 10$									
SNR	-20	-15	-10	-5	0	5	10	15	20
Simulation	0.33	0.34	0.34	0.35	0.39	0.43	0.56	0.66	0.76
Upper bound	0.33	0.33	0.34	0.35	0.39	0.44	0.56	0.68	0.77
Lower bound	0.33	0.33	0.34	0.35	0.38	0.44	0.55	0.65	0.74

Table 6. Analytic performance and simulated performance for all the targets in Fig. 4 (numerical values).

$\theta = 20°$, $M_1 = 6$, $M_2 = 12$, $M_3 = 10$, $M_4 = 12$									
SNR	-20	-15	-10	-5	0	5	10	15	20
Simulation	0.25	0.26	0.26	0.26	0.31	0.45	0.71	0.94	0.99
Upper bound	0.28	0.28	0.28	0.3	0.35	0.47	0.72	0.94	0.99
Lower bound	0.19	0.19	0.2	0.22	0.26	0.32	0.6	0.94	0.99
$\theta = 40°$, $M_1 = 6$, $M_2 = 12$, $M_3 = 10$, $M_4 = 12$									
SNR	-20	-15	-10	-5	0	5	10	15	20
Simulation	0.25	0.25	0.26	0.28	0.33	0.47	0.76	0.96	0.99
Upper bound	0.28	0.28	0.28	0.3	0.36	0.51	0.77	0.96	0.99
Lower bound	0.19	0.2	0.21	0.24	0.29	0.35	0.65	0.96	0.99
$\theta = 60°$, $M_1 = 6$, $M_2 = 12$, $M_3 = 10$, $M_4 = 12$									
SNR	-20	-15	-10	-5	0	5	10	15	20
Simulation	0.25	0.25	0.26	0.28	0.32	0.43	0.68	0.88	0.97
Upper bound	0.28	0.28	0.28	0.3	0.34	0.47	0.72	0.89	0.97
Lower bound	0.19	0.19	0.21	0.23	0.28	0.33	0.55	0.85	0.97
$\theta = 80°$, $M_1 = 6$, $M_2 = 12$, $M_3 = 10$, $M_4 = 12$									
SNR	-20	-15	-10	-5	0	5	10	15	20
Simulation	0.24	0.24	0.25	0.27	0.29	0.37	0.51	0.67	0.79
Upper bound	0.28	0.28	0.28	0.29	0.32	0.39	0.53	0.68	0.8
Lower bound	0.19	0.19	0.2	0.22	0.26	0.31	0.44	0.65	0.76

with $M_1 = 6$, $M_2 = 12$, $M_3 = 10$ and $M_4 = 12$. It is shown that the scheme presented in the paper can result in fairly good lower and upper bounds of the performance for multiple targets.

6. CONCLUSIONS

We considered the performance analysis of radar target recognition using natural frequency in the frequency domain. We extended the formulation in [5] to the frequency domain. The performance analysis based on the numerical evaluation of the probability density function (PDF) is presented. The derivation of the PDF is validated by comparing the analytical performance with the performance based on the Monte-Carlo simulation. To show the agreement between the analytic and simulated results, the frequency responses of simple targets are used. The results for two targets and multiple targets show that the scheme presented in this paper can be used for the performance analysis of the natural frequency-based radar target recognition in the frequency domain.

REFERENCES

1. Chen, J., S. Quegan, and X. Yin, "Calibration of spaceborne linearly polarized low frequency SAR using polarimetric selective radar calibrators," *Progress In Electromagnetics Research*, Vol. 114, 89–111, 2011.

2. Crowgey, B. R., E. J. Rothwell, L. C. Kempel, and E. L. Mokole, "Comparison of UWB short-pulse and stepped-frequency radar systems for imaging through barriers," *Progress In Electromagnetics Research*, Vol. 110, 403–419, 2010.

3. Park, J.-I. and K.-T. Kim, "A Comparative study on ISAR imaging algorithms for radar target identification," *Progress In Electromagnetics Research*, Vol. 108, 155–175, 2010.

4. Crocco, L., F. Soldovieri, T. Millington, and N. J. Cassidy, "Bistatic tomographic GPR imaging for incipient pipeline leakage evaluation," *Progress In Electromagnetics Research*, Vol. 101, 307–321, 2010.

5. Lazaro, A., D. Girbau, and R. Villarino, "Analysis of vital signs monitoring using an IR-UWB radar," *Progress In Electromagnetics Research*, Vol. 100, 265–284, 2010.

6. Cheng, X., H. Chen, X.-M. Zhang, B. Zhang, and B.-I. Wu, "Cloaking a perfectly conducting sphere with rotationally uniaxial nihility media in monostatic radar system," *Progress In Electromagnetics Research*, Vol. 100, 285–298, 2010.

7. Conceicao, R. C., M. O'Halloran, E. Jones, and M. Glavin, "Investigation of classifiers for early-stage breast cancer based on radar target signatures," *Progress In Electromagnetics Research*, Vol. 105, 295–311, 2010.

8. Bellomo, L., S. Pioch, M. Saillard, and E. Spano, "Time reversal experiments in the microwave range: Description of the radar and results," *Progress In Electromagnetics Research*, Vol. 104, 427–448, 2010.

9. Oraizi, H., A. Abdolali, and N. Vaseghi, "Application of double zero metamaterials as radar absorbing materials for the reduction of radar cross section," *Progress In Electromagnetics Research*, Vol. 101, 323–337, 2010.

10. Alexopoulos, A., "Effect of atmospheric propagation in RCS predictions," *Progress In Electromagnetics Research*, Vol. 101, 277–290, 2010.

11. Li, S., Y. Tian, G. Lu, Y. Zhang, H. J. Xue, J.-Q. Wang, and X.-J. Jing, "A new kind of non-acoustic speech acquisition method based on millimeter wave radar," *Progress In Electromagnetics Research*, Vol. 130, 17–40, 2012.

12. Burgos-Garcia, M., F. Perez-Martinez, and J. Gismero Menoyo, "Radar signature of a helicopter illuminated by a long LFM signal," *IEEE Transactions on Aerospace and Electronic Systems*, Vol. 45, 1104–1110, 2009.

13. Hong, S., L. Wang, Z.-G. Shi, and K. S. Chen, "Simplified particle PHD filter for multiple-target tracking: Algorithm and architecture," *Progress In Electromagnetics Research*, Vol. 120, 481–498, 2011.

14. Tian, B., D.-Y. Zhu, and Z.-D. Zhu, "A novel moving target detection approach for dual-channel SAR system," *Progress In Electromagnetics Research*, Vol. 115, 191–206, 2011.

15. Davy, M., T. Lepetit, J. de Rosny, C. Prada, and M. Fink, "Detection and imaging of human beings behind a wall using the dort method," *Progress In Electromagnetics Research*, Vol. 110, 353–369, 2010.

16. Ray, P. and P. K. Varshney, "Radar target detection framework based on false discovery rate," *IEEE Transactions on Aerospace and Electronic Systems*, Vol. 47, 1277–1292, 2011.

17. Zhou, S. H. and H. W. Liu, "Signal fusion-based target detection algorithm for spatial diversity radar," *IET Radar, Sonar and Navigation*, Vol. 5, 204–214, 2011.

18. Akakaya, M. and A. Nehorai, "MIMO radar detection and adaptive design under a phase synchronization mismatch," *IEEE Transactions on Signal Processing*, Vol. 58, 4994–5005, 2010.

19. Manasse, R., "Idealized bistatic radar GMTI detection with space-time processing," *IEEE Transactions on Aerospace and Electronic Systems*, Vol. 46, 1996–2003, 2010.

20. He, Q., N. H. Lehmann, R. S. Blum, and A. M. Haimovich, "MIMO radar moving target detection in homogeneous clutter," *IEEE Transactions on Aerospace and Electronic Systems*, Vol. 46, 1290–1301, 2010.

21. Yuan, C. C., F. Pascal, J.-P. Ovarlez, and M. Lesturgie, "MIMO radar detection in non-gaussian and heterogeneous clutter," *IEEE Journal of Selected Topics in Signal Processing*, Vol. 4, 115–126, 2010.

22. Budillon, A., A. Evangelista, and G. Schirinzi, "GLRT detection of moving targets via multibaseline along-track interferometric SAR systems," *IEEE Geoscience and Remote Sensing Letters*, Vol. 9, 348–352, 2012.

23. Guan, J., X.-L. Chen, Y. Huang, and Y. He, "Adaptive fractional fourier transform-based detection algorithm for moving target in heavy sea clutter," *IET Radar, Sonar and Navigation*, Vol. 6, 389–401, 2012.

24. Debes, C., A. M. Zoubir, and M. G. Amin, "Enhanced detection using target polarization signatures in through-the-wall radar imaging," *IEEE Transactions on Geoscience and Remote Sensing*, Vol. 50, 1968–1979, 2012.

25. Zhang, H., S. Y. Tan, and H. S. Tan, "Experimental study on a flanged parallel-plate dielectric waveguide probe for detection of buried inclusions," *Progress In Electromagnetics Research*, Vol. 111, 91–104, 2011.

26. Wang, X., J.-F. Chen, Z.-G. Shi, and K. S. Chen, "Fuzzy-control-based particle filter for maneuvering target tracking," *Progress In Electromagnetics Research*, Vol. 118, 1–15, 2011.

27. Mao, X., D.-Y. Zhu, L. Ding, and Z.-D. Zhu, "Comparative study of RMA and PFA on their responses to moving target," *Progress*

In Electromagnetics Research, Vol. 110, 103–124, 2010.

28. Sjogren, T. K., V. T. Vu, M. I. Pettersson, A. Gustavsson, and L. M. H. Ulander, "Moving target relative speed estimation and refocusing in synthetic aperture radar images," *IEEE Transactions on Aerospace and Electronic Systems*, Vol. 48, 2426–2436, 2012.

29. Hassanien, A., S. A. Vorobyov, and A. B. Gershman, "Moving target parameters estimation in noncoherent MIMO radar systems," *IEEE Transactions on Signal Processing*, Vol. 60, 2354–2361, 2012.

30. Gao, P. C., Y. B. Tao, and H. Lin, "Fast RCS prediction using multiresolution shooting and bouncing ray method on the GPU," *Progress In Electromagnetics Research*, Vol. 107, 187–202, 2010.

31. Garcia-Donoro, D., I. Martinez-Fernandez, L. E. Garcia-Castillo, Y. Zhang, and T. K. Sarkar, "RCS computation using a parallel in-core and out-of-core direct solver," *Progress In Electromagnetics Research*, Vol. 118, 505–525, 2011.

32. Xu, H.-Y., H. Zhang, K. Lu, and X.-F. Zeng, "A holly-leaf-shaped monopole antenna with low RCS for UWB application," *Progress In Electromagnetics Research*, Vol. 117, 35–50, 2011.

33. De Cos, M. E., Y. Alvarez Lopez, and F. Las-Heras, "On the influence of coupling amc resonances for RCS reduction in the SHF band," *Progress In Electromagnetics Research*, Vol. 117, 103–119, 2011.

34. Bennani, Y., F. Comblet, and A. Khenchaf, "RCS of complex targets: Original representation validated by measurements application to ISAR imagery," *IEEE Transactions on Geoscience and Remote Sensing*, Vol. 50, 3882–3891, 2012.

35. Sirenko, K., V. Pazynin, Y. K. Sirenko, and H. Baci, "Compression and radiation of high-power short RF pulses. II. A novel antenna array design with combined compressor/radiator elements," *Progress In Electromagnetics Research*, Vol. 116, 271–296, 2011.

36. Li, J., B. Wei, Q. He, L.-X. Guo, and D.-B. Ge, "Time-domain iterative physical optics method for analysis of EM scattering from the target half buried in rough surface: PEC case," *Progress In Electromagnetics Research*, Vol. 121, 391–408, 2011.

37. Jandieri, V., K. Yasumoto, and Y.-K. Cho, "Rigorous analysis of electromagnetic scattering by cylindrical EBG structures," *Progress In Electromagnetics Research*, Vol. 121, 317–342, 2011.

38. Lin, G.-R., F.-S. Meng, and Y.-H. Lin, "Second-order scattering

induced reflection divergence and nonlinear depolarization on randomly corrugated semiconductor nano-pillars," *Progress In Electromagnetics Research*, Vol. 117, 67–81, 2011.

39. Cui, Z., Y. Han, C. Y. Li, and W. Zhao, "Efficient analysis of scattering from multiple 3-D cavities by means of a FE-BI-DDM method," *Progress In Electromagnetics Research*, Vol. 116, 425–439, 2011.

40. Jiang, W.-Q., M. Zhang, H. Chen, and Y.-G. Lu, "CUDA implementation in the EM scattering of a three-layer canopy," *Progress In Electromagnetics Research*, Vol. 116, 457–473, 2011.

41. Du, Y., W.-Z. Yan, J.-C. Shi, Z. Li, and E.-X. Chen, "Electromagnetic scattering from a corn canopy at L and C bands," *Progress In Electromagnetics Research*, Vol. 114, 33–49, 2011.

42. Valagiannopoulos, C. A., "Electromagnetic scattering of the field of a metamaterial slab antenna by an arbitrarily positioned cluster of metallic cylinders," *Progress In Electromagnetics Research*, Vol. 114, 51–66, 2011.

43. Litman, A., J.-M. Geffrin, and H. Tortel, "On the calibration of a multistatic scattering matrix measured by a fixed circular array of antennas," *Progress In Electromagnetics Research*, Vol. 110, 1–21, 2010.

44. Hellicar, A. D., J. S. Kot, G. C. James, and G. K. Cambrell, "The analysis of 3D model characterization and its impact on the accuracy of scattering calculations," *Progress In Electromagnetics Research*, Vol. 110, 125–145, 2010.

45. Bucinskas, J., L. Nickelson, and V. Shugurovas, "Microwave scattering and absorption by a multilayered lossy metamaterial — Glass cylinder," *Progress In Electromagnetics Research*, Vol. 105, 103–118, 2010.

46. Ding, D.-Z. and R.-S. Chen, "Electromagnetic scattering by conducting bor coated with chiral media above a lossy half-space," *Progress In Electromagnetics Research*, Vol. 104, 385–401, 2010.

47. Mittal, G. and D. Singh, "Critical analysis of microwave specular scattering response on roughness parameter and moisture content for bare periodic rough surfaces and its retrieval," *Progress In Electromagnetics Research*, Vol. 100, 129–152, 2010.

48. Caramanica, F. and G. Oliveri, "An innovative multi-source strategy for enhancing the reconstruction capabilities of inverse scattering techniques," *Progress In Electromagnetics Research*, Vol. 101, 349–374, 2010.

49. Li, J., L.-X. Guo, and H. Zeng, "FDTD method investigation on the polarimetric scattering from 2-D rough surface," *Progress In Electromagnetics Research*, Vol. 101, 173–188, 2010.

50. Chang, Y.-L., C.-Y. Chiang, and K.-S. Chen, "SAR image simulation with application to target recognition," *Progress In Electromagnetics Research*, Vol. 119, 35–57, 2011.

51. Lui, H.-S. and N. V. Shuley, "Resonance based target recognition using ultrawideband polarimetric signatures," *IEEE Transactions on Antennas and Propagation*, Vol. 60, 3985–3988, 2012.

52. Du, L., H. Liu, P. Wang, B. Feng, M. Pan, and Z. Bao, "Noise robust radar HRRP target recognition based on multitask factor analysis with small training data size," *IEEE Transactions on Signal Processing*, Vol. 60, 3546–3559, 2012.

53. Smith, G. E. and B. G. Mobasseri, "Robust through-the-wall radar image classification using a target-model alignment procedure," *IEEE Transactions on Image Processing*, Vol. 21, 754–767, 2012.

54. Zhang, H., N. M. Nasrabadi, Y. Zhang, and T. S. Huang, "Multi-view automatic target recognition using joint sparse representation," *IEEE Transactions on Aerospace and Electronic Systems*, Vol. 48, 2481–2497, 2012.

55. Chamberlain, N. E., E. K. Walton, and F. D. Garber, "Radar target identification of aircraft using polarization-diverse features," *IEEE Transactions on Aerospace and Electronic Systems*, Vol. 27, 58–67, 1991.

56. Aldhubaib, F. and N. V. Shuley, "Radar target recognition based on modified characteristic polarization states," *IEEE Transactions on Aerospace and Electronic Systems*, Vol. 46, 1921–1933, 2010.

57. Du, L., H. Liu, Z. Bao, and M. Xing, "Radar HRRP target recognition based on higher order spectra," *IEEE Transactions on Signal Processing*, Vol. 53, 2359–2368, 2005.

58. Du, L., H. Liu, P. Wang, B. Feng, M. Pan, and Z. Bao, "Noise robust radar HRRP target recognition based on multitask factor analysis with small training data size," *IEEE Transactions on Signal Processing*, Vol. 60, 3546–3559, 2012.

59. Du, L., P. Wang, H. Liu, M. Pan, F. Chen, and Z. Bao, "Bayesian spatiotemporal multitask learning for radar HRRP target recognition," *IEEE Transactions onSignal Processing*, Vol. 59, 3182–3196, 2011.

60. Tesche, F., "On the analysis of scattering and antenna problem using the singularity expansion method," *IEEE Transactions on*

Antennas and Propagation, Vol. 21, 53–62, Jan. 1973.

61. Baum, C., E. Rothwell, K. Chen, and D. Nyquist, "The singularity expansion method and its application to target identification," *Proceedings of the IEEE*, Vol. 79, 1481–1492, Oct. 1991.

62. Lee, J.-H. and H.-T. Kim, "Radar target recognition based on late time representation: Closed-form expression for criterion," *IEEE Transactions on Antennas and Propagation*, Vol. 54, 2455–2462, Sep. 2006.

63. Lee, J.-H. and H.-T. Kim, "Radar target recognition using least squares estimate," *Microwave and Optical Technology Letters*, Vol. 30, 427–434, Sep. 2001.

64. Mooney, J. E., Z. Ding, and L. S. Riggs, "Performance analysis of a GLRT automated target discrimination scheme," *IEEE Transactions on Antennas and Propagation*, Vol. 49, No. 12, 1827–1835, Dec. 2001.

65. Han, S.-K., H.-T. Kim, S.-H. Park, and K.-T. Kim, "Efficient radar target recognition using a combination of range profile and time-frequency analysis," *Progress In Electromagnetics Research*, Vol. 108, 131–140, 2010.

66. Huang, C.-W. and K.-C. Lee, "Application of ica technique to PCA based radar target recognition," *Progress In Electromagnetics Research*, Vol. 105, 157–170, 2010.

67. Morales, J. D., D. Blanco, D. P. Ruiz, and M. C. Carrion, "Non cooperative radar target identification using exponential single-mode extraction pulse," *IEEE Transactions on Antennas and Propagation*, Vol. 59, No. 6, 2445–2447, 2011

68. Lee, W., T. K. Sarkar, H. Moon, and L. Brown, "Detection and identification using natural frequency of the perfect electrically conducting (PEC) sphere in the frequency and time domain," *IEEE International Symposium on Antennas and Propagation*, 2334–2337, 2011

69. Chauveau, J., N. de Beaucoudrey, and J. Saillard, "Resonance behavior of radar targets with aperture: Example of an open rectangular cavity," *IEEE Transactions on Antennas and Propagation* Vol. 58, No. 6, 2060–2068, 2010.

70. Aldhubaib, F., H.-S. Lui, and N. V. Shuley, "A radar target signature based on resonance and dual polarization features," *Microwave Conference*, 1–4, 2008.

71. Wang, M.-J., Z.-S. Wu, Y.-L. Li, and G. Zhang, "High resolution range profile identifying simulation of laser radar based on pulse beam scattering characteristics of targets," *Progress In*

Electromagnetics Research, Vol. 96, 193–204, 2009.

72. Jia, Y., L. Kong, and X. Yang, "A novel approach to target localization through unknown walls for through-the-wall radar imaging," *Progress In Electromagnetics Research*, Vol. 119, 107–132, 2011.

73. Diao, W.-H., X. Mao, and V. Gui, "Metrics for performance evaluation of preprocessing algorithms in infrared small target images," *Progress In Electromagnetics Research*, Vol. 115, 35–53, 2011.

74. Zhang, M., Y. W. Zhao, H. Chen, and W.-Q. Jiang, "SAR imaging simulation for composite model of ship on dynamic ocean scene," *Progress In Electromagnetics Research*, Vol. 113, 395–412, 2011.

75. Wei, S.-J., X.-L. Zhang, J. Shi, and G. Xiang, "Sparse reconstruction for SAR imaging based on compressed sensing," *Progress In Electromagnetics Research*, Vol. 109, 63–81, 2010.

76. Xu, W., P. Huang, and Y.-K. Deng, "MIMO-Tops mode for high-resolution ultra-wide-swath full polarimetric imaging," *Progress In Electromagnetics Research*, Vol. 121, 19–37, 2011.

77. Huang, Y., P. V. Brennan, D. Patrick, I. Weller, P. Roberts, and K. Hughes, "FMCW based MIMO imaging radar for maritime navigation," *Progress In Electromagnetics Research*, Vol. 115, 327–342, 2011.

78. Jin, Y.-Q., "Polarimetric scattering modeling and information retrieval of SAR remote sensing — A review of FDU work," *Progress In Electromagnetics Research*, Vol. 104, 333–384, 2010.

79. Qi, Y., W. Tan, Y. Wang, W. Hong, and Y. Wu, "3D bistatic omega-k imaging algorithm for near range microwave imaging systems with bistatic planar scanning geometry," *Progress In Electromagnetics Research*, Vol. 121, 409–431, 2011.

80. Xin, Y. H., Y. Z. Xiao, and J. C. Tie, "Fast 3D-ISAR image simulation of targets at arbitrary aspect angles through nonuniform fast Fourier transform (NUFFT)," *IEEE Transactions on Antennas and Propagation*, Vol. 60, 2597–2602, 2012.

81. Lei, Z., Z.-J. Qiao, M.-D. Xing, J.-L. Sheng, R. Guo, and Z. Bao, "High-resolution ISAR imaging by exploiting sparse apertures," *IEEE Transactions on Antennas and Propagation*, Vol. 60, 997–1008, 2012.

82. Abe, Y., S. Kidera, and T. Kirimoto, "Accurate and omnidirectional UWB radar imaging algorithm with RPM method extended to curvilinear scanning model," *IEEE Geoscience and Remote Sensing Letters*, Vol. 9, 144–148, 2012.

83. Buddendick, H. and T. F. Eibert, "Bistatic image formation from shooting and bouncing rays simulated current distributions," *Progress In Electromagnetics Research*, Vol. 119, 1–18, 2011.

84. Lim, H. and N.-H. Myung, "A novel hybrid AIPO-MoM technique for jet engine modulation analysis," *Progress In Electromagnetics Research*, Vol. 104, 85–97, 2010.

85. Chen, J., Z. Li, and C.-S. Li, "A novel strategy for topside ionosphere sounder based on spaceborne MIMO radar with FDCD," *Progress In Electromagnetics Research*, Vol. 116, 381–393, 2011.

86. Bullard, B. D. and P. C. Dowdy, "Pulse doppler signature of a rotary-wing aircraft," *IEEE Aerospace and Electronic Systems Magazine*, Vol. 6, 28–30, 1991.

87. Yoon, S.-H., B. Kim, and Y.-S. Kim, "Helicopter classification using time-frequency analysis," *Electronics Letters*, Vol. 36, 1871–1872, 2000.

88. Ji, W.-J. and C.-M. Tong, "Bistatic scattering from two-dimensional dielectric ocean rough surface with a PEC object partially embedded by using the G-SMCG method," *Progress In Electromagnetics Research*, Vol. 105, 119–139, 2010.

89. Sun, J., S. Mao, G. Wang, and W. Hong, "Polar format algorithm for spotlight bistatic SAR with arbitrary geometry configuration," *Progress In Electromagnetics Research*, Vol. 103, 323–338, 2010.

90. Crocco, L., F. Soldovieri, T. Millington, and N. J. Cassidy, "Bistatic tomographic GPR imaging for incipient pipeline leakage evaluation," *Progress In Electromagnetics Research*, Vol. 101, 307–321, 2010.

91. Wu, J., J. Yang, Y. Huang, Z. Liu, and H. Yang, "A new look at the point target reference spectrum for bistatic SAR," *Progress In Electromagnetics Research*, Vol. 119, 363–379, 2011.

92. Sirenko, K., V. Pazynin, Y. K. Sirenko, and H. Baci, "Compression and radiation of high-power short RF pulses. I. Energy accumulation in direct-flow waveguide compressors," *Progress In Electromagnetics Research*, Vol. 116, 239–270, 2011.

93. Galati, G. and G. Pavan, "Range sidelobes suppression in pulse-compression radar using Golay pairs: Some basic limitations for complex targets," *IEEE Transactions on Aerospace and Electronic Systems*, Vol. 48. 2756–2760, 2012.

94. Akbaripour, A. and M. H. Bastani, "Range sidelobe reduction filter design for binary coded pulse compression system," *IEEE Transactions on Aerospace and Electronic Systems*, Vol. 48, 348–

359, 2012.

95. Li, L., A. E.-C. Tan, K. Jhamb, and K. Rambabu, "Buried object characterization using ultra-wideband ground penetrating radar," *IEEE Transactions on Microwave Theory and Techniques*, Vol. 60, 2654–2664, 2012.

96. Zhu, C.-H., Q. H. Liu, Y. Liu, Y. Shen, and L. J. Liu, "An accurate conformal Fourier transform method for 2D discontinuous functions," *Progress In Electromagnetics Research*, Vol. 120, 165–179, 2011.

97. Zhu, C.-H., Q. H. Liu, Y. Shen, and L. Liu, "A high accuracy conformal method for evaluating the discontinuous Fourier transform," *Progress In Electromagnetics Research*, Vol. 109, 425–440, 2010.

98. Horn, R. A. and C. R. Johnson, *Matrix Analysis*, Cambridge University Press, Cambridge, UK, 1986.